

Experimental lower bounds on entanglement entropy without twin copy

Yannick Meurice

Department of Physics and Astronomy, The University of Iowa, Iowa City, IA 52242, USA

(Dated: July 16, 2024)

We discuss the possibility of estimating experimentally the von Neumann entanglement entropy S_A^{vN} of a symmetric bi-partite quantum system AB by using the basic measurement counts for a *single* copy of a prepared state. Using exact diagonalization and analog simulations performed with the publicly available QuEra facilities for chains and ladders of Rydberg atoms, we calculate the Shannon entropy S_{AB}^X associated with the experimental measurements of adiabatically prepared ground states and the reduced entropy S_A^X obtained by tracing the experimental probabilities over the B half of the system. We show several examples for which, in good approximation, $S_A^{vN} \propto (2S_A^X - S_{AB}^X)$ with a constant of proportionality slightly larger than one. We argue that one should have the inequality $S_A^{vN} \geq (2S_A^X - S_{AB}^X)$ holding in more general circumstances. $2S_A^X - S_{AB}^X$ can be calculated easily for many qubit platforms and appears to be generically robust under measurement errors. Similar results are found for the second order Rényi entanglement entropy.

Motivations. Entanglement entropy is a crucial theoretical concept in quantum physics with applications for many-body physics [1–4], gauge theory [5–8], high-energy collisions [9–11], nuclear physics [12, 13] and studies of conformal field theory [14–17]. It provides important information regarding quantum phases transitions. However, the experimental measurement of entanglement entropy is notoriously difficult due to its nonlocal nature. This led to the idea of coupling several copies of the original system [18]. A standard proposal is to measure the second order Rényi entropy S_2 by performing a swap operation between twin copies of a system [19]. Cold atom experimentalists [20, 21] were able to prepare and interfere twin copies of a state in small optical lattices to measure S_2 . If practically feasible for larger systems, this would allow the experimental measurement of the central charge which is an important characterization of conformal systems [14–16, 22].

Bitstring probabilities. Preparing and interfering twin copies of a quantum system are not easy experimental tasks. On the other hand, a generic qubit-based quantum computing device provides experimental counts for bitstrings typically provided as python dictionaries. For instance, for 1000 shots with a two-qubit universal quantum computer one gets counts for the four possible states in the form {'01': 269, '00': 251, '10': 247, '11': 233}.

As another example, for a 10 Rydberg atom analog simulator where g and r represent, for each atom, the ground and Rydberg states respectively the counts are given as {'gggrgrgrgr': 8, 'rgrgrgrgr': 160, ...}. By dividing these counts by the total number of shots, we can estimate the probabilities $p_{\{n\}}$ for the bitstring states $|\{n\}\rangle$. In this article, we propose to use proxy quantities calculated from the $p_{\{n\}}$ from a single copy to estimate the entanglement entropy.

Bipartite setup. We consider a bipartite quantum system AB made out of two parts A and B . For simplicity, we assume that A and B have the same size and can

be interchanged by a reflection symmetry. We use a pure state density matrix ρ_{AB} , the reduced $\rho_A = \text{Tr}_B \rho_{AB}$ and the usual von Neumann entanglement entropy

$$S_A^{vN} \equiv -\text{Tr}(\rho_A \ln(\rho_A)), \quad (1)$$

which is independent of the basis used in A . The Shannon entropy for the experimental probabilities is:

$$S_{AB}^X \equiv -\sum_{\{n\}} p_{\{n\}} \ln(p_{\{n\}}). \quad (2)$$

The superscript X is short for eXperimental as opposed to von Neuman (or Rényi). As explained in a more systematic way in SM II.A [23], we assume that the computational basis has a bipartite factorization $|\{n\}_{AB}\rangle = |\{n\}_A\rangle |\{n\}_B\rangle$ and that we can define reduced probabilities by tracing over one half of the system:

$$p_{\{n\}_A} = \sum_{\{n\}_B} p_{\{n\}_A \{n\}_B}. \quad (3)$$

This leads to the reduced experimental entropy

$$S_A^X \equiv -\sum_{\{n\}_A} p_{\{n\}_A} \ln(p_{\{n\}_A}). \quad (4)$$

A first guess. It is straightforward to calculate S_{AB}^X and S_A^X from output dictionaries but these quantities depend strongly on the computational basis and do not provide unique characterizations of the system. On the other hand, given our assumptions, we see that for a uniform product state $S_{AB}^X = 2S_A^X$. Our first guess is that the difference between these two quantities could be used to estimate the basis-independent entanglement between A and B , namely

$$S_A^{vN} \propto 2S_A^X - S_{AB}^X. \quad (5)$$

We will show with some examples that this can be verified in good approximation and that basis-dependent features

as well as measurement errors tend to cancel in this specific linear combination. Experimental probabilities for a single copy are available on many analog and universal quantum computing platforms. In the following, we focus on configurable arrays of Rydberg atoms. We conducted experimental analog simulations using the QuEra device Aquila [24] which is publicly available.

Rydberg atoms setup. Recently, optical tweezers have been used to create arrays of Rydberg atoms with adjustable geometries [25–30]. Their Hamiltonian reads

$$H = \frac{\Omega}{2} \sum_i (|g_i\rangle \langle r_i| + |r_i\rangle \langle g_i|) - \Delta \sum_i n_i + \sum_{i < j} V_{ij} n_i n_j, \quad (6)$$

with van der Waals interactions $V_{ij} = \Omega R_b^6 / r_{ij}^6$, for a distance r_{ij} between the atoms labelled as i and j . By definition, $r_{ij} = R_b$, the Rydberg blockade radius, when $V_{ij} = \Omega$ the Rabi frequency. We define the Rydberg occupation $n_i |r_i\rangle = |r_j\rangle$ while $n_i |g_i\rangle = 0$. In the following we use $\Omega = 5\pi$ MHz, which implies $R_b = 8.375\mu$, and a detuning $\Delta = 17.5\pi$ MHz as in [31]. We will consider chains and ladders of atoms with varying lattice spacings. Note that in Ref. [31], one can see precise correspondence between the contour plots in the $\Delta/\Omega - R_b/a$ plane of the peak height of the structure factors, which can be reconstructed from the basis dependent $p_{\{n\}}$ only, and the contour plots of S_A^{vN} .

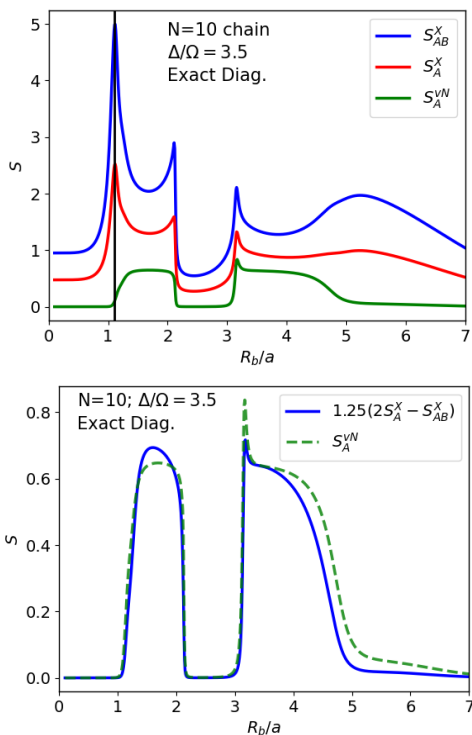


FIG. 1. Entropies for a chain of 10 atoms with $\Delta/\Omega = 3.5$ as a function of R_b/a_x . Top: S_{AB}^X , S_A^X and S_A^{vN} ; the vertical line is at $R_b/a_x = 1.11$; Bottom: $1.25(2S_A^X - S_{AB}^X)$ and S_A^{vN} .

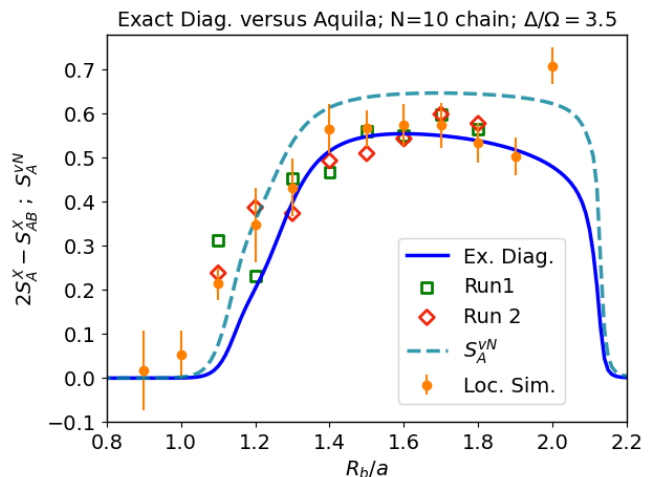


FIG. 2. $2S_A^X - S_{AB}^X$ vs. R_b/a_x with three methods: 1) exact diagonalization (continuous curve); 2) local simulator with no ramping down of Ω at the end (filled circles), the errors bars are calculated using 10 independent runs of 1000 shots; 3) 2 runs with 1000 shots with Aquila (empty symbols); S_A^{vN} (dashed line) is also given for reference.

Numerical calculations. A first illustration of Eq. (5) is obtained by using the ground state of a chain of 10 Rydberg atoms separated by a varied lattice spacing a_x expressed in units of R_b . We used exact diagonalization to calculate S_{AB}^X , S_A^X and S_A^{vN} for the vacuum. The results are shown in Fig. 1. We observe that $S_A^{vN} \simeq 1.25(2S_A^X - S_{AB}^X)$. The proportionality is only approximate, for instance, S_A^{vN} is slightly below (above) this linear combination for smaller (larger) R_b/a_x respectively. Notice that as R_b/a_x is increased from low values, the onset of S_A^{vN} is marked by a sharp increase S_{AB}^X and S_A^X . However, at the peak of S_{AB}^X and S_A^X , for $R_b/a_x \simeq 1.11$, cancellations occur and S_A^{vN} develops only after S_{AB}^X and S_A^X drop significantly. Other features of Fig. 1 can be understood from elementary considerations that are provided in SM II.B [23].

Analog calculations. We have repeated the above calculations using the Aquila device and the associated Amazon Braket local simulator. As explained in SM I [23], this imposes size constraints not present in exact diagonalization. Calculations for $1.0 \lesssim R_b/a_x \lesssim 2$ can be performed with the local simulator and, for a slightly shorter range of R_b/a_x , with Aquila. In both cases, we ramped up the vacuum adiabatically starting with all atoms in the atomic ground state, increasing Ω and then Δ , exactly as in [31] and illustrated in the Appendix. The results are shown in Fig. 2 where we see good experimental estimates of $2S_A^X - S_{AB}^X$ with Aquila. The local simulator becomes less accurate when $R_b/a_x \simeq 2$ and the ramping down of Ω at the end involves subtleties discussed in SI. E [23]. Fig. 2 only shows results with no ramping down of Ω at the end for the local simulator.

Error cancellations. An important aspect of the results presented in Fig. 2 is that the systematic errors of S_{AB}^X and S_A^X are significant. However these errors appear to cancel in $2S_A^X - S_{AB}^X$. This is discussed in SM II.E [23].

Limitations. So far Eq. (5) has been an unexpectedly successful guess. Fig. 1 shows clearly the approximate factor 2 relating the height of the peaks of S_{AB}^X and S_A^X and that no such peak appears in either side of Eq. (5). We do not have a general argument to show that this should hold in general. Actually, a simple counterexample where Eq. (5) does *not* hold can be found [32]: consider the density matrix for the two atom state with $S_A^{vN} = \ln 2$:

$$|ZX\rangle = \frac{1}{2}(|gg\rangle + |gr\rangle + |rg\rangle - |rr\rangle). \quad (7)$$

All the $p_{\{n\}}$ for this state are 1/4 and are identical to the $p_{\{n\}}$ for the $|XX\rangle$ product state where the coefficient of $|rr\rangle$ is +1 and $S_A^{vN} = 0$. For both states, $S_{AB}^X = 2S_A^X$ and clearly Eq. (5) does not hold for $|ZX\rangle$. More generally any proxy for S_A^{vN} which depends only on the $p_{\{n\}}$ has symmetries that are *not* symmetries of S_A^{vN} . In the above example, $|ZX\rangle$ can be obtained from $|XX\rangle$ by applying the entangling unitary transformation $\exp(i\pi n_1 n_2)$ which is a symmetry of the $p_{\{n\}}$ but not of S_A^{vN} .

An improved guess. The above counterexample suggests that Eq. (5) can only *partially* capture the entanglement and that it should be replaced by the inequality

$$S_A^{vN} \geq 2S_A^X - S_{AB}^X. \quad (8)$$

Fig. 3 shows that this inequality is verified for chains of size $N_s = 2, 4, \dots, 10$. For $N_s = 10$, the fraction of S_A^{vN} not accounted by $2S_A^X - S_{AB}^X$ is compatible with the proportionality factor 1.25 used previously. In the case

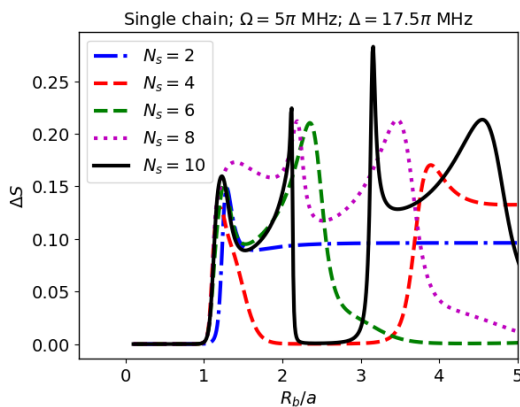


FIG. 3. $S_A^{vN} - (2S_A^X - S_{AB}^X)$ as a function of R_b/a_x for chains of size $N_s = 2, 4, \dots, 10$.

of two qubits, it is possible to show that the inequality (8) holds in general. The details are shown in SM II. D

[23]. We first show that S^{vN} depends on the $|c_{n_1 n_2}|$ and a single angle ξ and that

$$S^{vN}(|c_{n_1 n_2}\rangle, \xi) \geq S^{vN}(|c_{n_1 n_2}\rangle, \xi = 0) \geq 2S_A^X - S_{AB}^X. \quad (9)$$

The second inequality is verified in Fig. 4 using spherical coordinates to parametrize the norms of the coefficients expressed in spherical coordinates $|c_{00}| = \cos \phi \sin \theta$; $|c_{11}| = \sin \phi \sin \theta$; $|c_{01}| = |c_{10}| = \cos \theta / \sqrt{2}$ which imposes the constraint that the probabilities add to one.

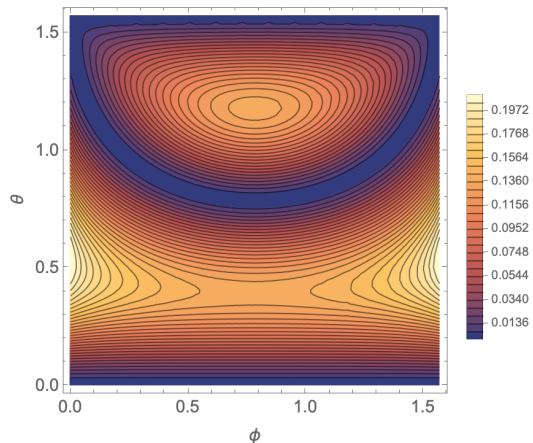


FIG. 4. $S^{vN}(\xi = 0) - (2S_A^X - S_{AB}^X)$ for two qubits using the spherical coordinates described in the text.

Other numerical examples. It is easy to illustrate Eqs. (5) and (8) with other geometries. We have considered two-leg ladders with five rungs and varied lattice spacing in both directions. We observed similar features shown in SM II.C [23]. Again the approximate constant of proportionality 1.25 was used to display both quantities in the same figure. The approximate constant of proportionality depends on Ω/Δ and does not appear to have any universal meaning.

Rényi entropy. One can easily construct an experimental second order Rényi version of the S^X quantities defined above:

$$S_{2AB}^X \equiv -\ln \sum_{\{n\}} p_{\{n\}}^2, \text{ and } S_{2A}^X \equiv -\ln \sum_{\{n\}_A} p_{\{n\}_A}^2. \quad (10)$$

As shown in SM II.F [23], we found a very similar result for the 10 atom chain using exact diagonalization:

$$S_{2A}^R \propto 2S_{2A}^X - S_{2AB}^X. \quad (11)$$

with $S_{2A}^R = -\ln(\text{Tr} \rho_A^2)$.

Configurational entanglement entropy. The connection between correlations and purity [33] or the reconstruction of quantum states using a restricted Boltzmann machine based on single-basis measurements [34] could help develop a more general understanding of our

observations. Ref. [33] introduces another proxy C for S_A^{vN} in the case of the the Bose-Hubbard model called the configurational entanglement entropy. Adapting their definition for the case where the particle number is not conserved and where there is no number entropy, and introducing a function of C that reproduces S_A^{vN} for a two-qubit Bell state we propose to use

$$LC \equiv \ln\left(1 + \sum_{\{n\}} |p_{\{n\}} - p_{\{n\}_A} p_{\{n\}_B}|\right). \quad (12)$$

This quantity provides good estimates of S_A^{vN} but has a more intricate behavior which will be discussed separately.

Applications. Arrays of Rydberg atoms have been proposed for quantum simulation of lattice gauge theories [35–44]. More specifically, ladder arrays have been considered as quantum simulators for scalar electrodynamics [39] and their phase diagram have been studied experimentally [31] and with effective Hamiltonian methods [45]. These results show a very rich phase diagram and the need to study the regions of parameter spaces where the correlation lengths are much larger than the lattice spacing (continuum limits). This has possible relevance for the study of inhomogeneous phases and the Lifshitz regime of lattice quantum chromodynamics [46, 47]. Entanglement entropy considerations play an important role in the tentative designs of hybrid algorithms for collider event generators [42].

Generalizations. It is possible to extend our procedure for arbitrary AB partitions where, for instance, A and B have different sizes by replacing $2S_A^X$ by $S_A^X + S_B^X$ in Eq. (8) as in Shannon’s mutual information. This allows us to study the conjectured lower bound for multipartite entropies which are of great interest in the context of conformal field theory [48–50]. Ongoing calculations show that our proxy provide reasonably tight lower bounds for digitized ϕ^4 models with qudits [51], Ising models in curved space [52] and larger Rydberg arrays than the ones considered here [53].

Conclusions. We have provided Rydberg array examples where the von Neumann entanglement entropy S_A^{vN} can be estimated approximately from $2S_A^X - S_{AB}^X$ or two other proxy quantities inspired by the Rényi and configuration entropies. These proxies only depend on the $p_{\{n\}}$ and have symmetries that can conflict with completely capturing S_A^{vN} . We found clear indications that $2S_A^X - S_{AB}^X$ is a lower bound for S_A^{vN} . This was observed in all the examples where we made calculations and proven rigorously for a general two-qubit state. We are working on extending the proof of this statement to larger numbers of qubits. It is in principle possible to have entangled states not identified with the proxy as in the counterexample discussed here, however this situation seems atypical and in the sample calculations, missing a small fraction of the entanglement seems more

generic. $2S_A^X - S_{AB}^X$ can be calculated easily using the bitstring counts for a single copy of a system and is robust against systematic errors. This quantity provides a simple diagnosis to quickly identify regions of interest in a large space of adjustable parameters such as the lattice spacing or the detuning energy in our examples. The method can be applied to any qubit based universal or analog quantum computing device. We expect that this will lead to a broader set of supporting evidence for our observations and that it will stimulate the exploration of new quantum phases in analog simulators.

ACKNOWLEDGEMENTS

This research was supported in part by the Dept. of Energy under Award Number DE-SC0019139. Special thanks to Alex Lukin who pointed out the counterexample of Eq. (7) as well as the importance of understanding the proportionality factor. We thank S. Cantu, M. Asaduzzaman, J. Corona, Cheng Chin, Sheng-Tao Wang, A. Bylinskii, Fangli Liu, J. Zeiher, R. Pisarski, P. Komar and P. Preiss for comments and support. We thank the Amazon Web Services and S. Hassinger for facilitating remote access to QuEra through the Amazon Bracket while teaching quantum mechanics and our Department of Physics and Astronomy for supporting the cost of the analog simulations presented here.

-
- [1] L. Amico, R. Fazio, A. Osterloh, and V. Vedral, *Reviews of Modern Physics* **80**, 517 (2008).
 - [2] J. Eisert, M. Cramer, and M. B. Plenio, *Rev. Mod. Phys.* **82**, 277 (2010), arXiv:0808.3773 [quant-ph].
 - [3] D. A. Abanin, E. Altman, I. Bloch, and M. Serbyn, *Reviews of Modern Physics* **91** (2019), 10.1103/revmodphys.91.021001.
 - [4] J. I. Cirac, D. Perez-Garcia, N. Schuch, and F. Verstraete, *Rev. Mod. Phys.* **93**, 045003 (2021), arXiv:2011.12127 [quant-ph].
 - [5] S. Ghosh, R. M. Soni, and S. P. Trivedi, *JHEP* **09**, 069 (2015), arXiv:1501.02593 [hep-th].
 - [6] K. Van Acoleyen, N. Bultinck, J. Haegeman, M. Marien, V. B. Scholz, and F. Verstraete, *Phys. Rev. Lett.* **117**, 131602 (2016), arXiv:1511.04369 [quant-ph].
 - [7] M. C. Bañuls, K. Cichy, J. I. Cirac, K. Jansen, and S. Kühn, *Phys. Rev. X* **7**, 041046 (2017), arXiv:1707.06434 [hep-lat].
 - [8] J. Knaute, M. Feuerstein, and E. Zohar, *JHEP* **02**, 174 (2024), arXiv:2401.01930 [quant-ph].
 - [9] D. E. Kharzeev and E. M. Levin, *Phys. Rev. D* **95**, 114008 (2017), arXiv:1702.03489 [hep-ph].
 - [10] O. K. Baker and D. E. Kharzeev, *Phys. Rev. D* **98**, 054007 (2018).
 - [11] K. Zhang, K. Hao, D. Kharzeev, and V. Korepin, *Phys. Rev. D* **105**, 014002 (2022), arXiv:2110.04881 [quant-ph].

- [12] S. R. Beane, D. B. Kaplan, N. Klco, and M. J. Savage, *Phys. Rev. Lett.* **122**, 102001 (2019), arXiv:1812.03138 [nucl-th].
- [13] C. Robin, M. J. Savage, and N. Pillet, *Phys. Rev. C* **103**, 034325 (2021), arXiv:2007.09157 [nucl-th].
- [14] G. Vidal, J. I. Latorre, E. Rico, and A. Kitaev, *Phys. Rev. Lett.* **90**, 227902 (2003).
- [15] V. E. Korepin, *Phys. Rev. Lett.* **92**, 096402 (2004).
- [16] P. Calabrese and J. L. Cardy, *Int. J. Quant. Inf.* **4**, 429 (2006), arXiv:quant-ph/0505193.
- [17] S. Ryu and T. Takayanagi, *Phys. Rev. Lett.* **96**, 181602 (2006), arXiv:hep-th/0603001.
- [18] D. A. Abanin and E. Demler, *Phys. Rev. Lett.* **109**, 020504 (2012).
- [19] A. J. Daley, H. Pichler, J. Schachenmayer, and P. Zoller, *Phys. Rev. Lett.* **109**, 020505 (2012).
- [20] R. Islam, R. Ma, P. M. Preiss, M. Eric Tai, A. Lukin, M. Rispoli, and M. Greiner, *Nature* **528**, 77–83 (2015).
- [21] A. M. Kaufman, M. E. Tai, A. Lukin, M. Rispoli, R. Schittko, P. M. Preiss, and M. Greiner, *Science* **353**, 794–800 (2016).
- [22] J. Unmuth-Yockey, J. Zhang, P. M. Preiss, L.-P. Yang, S. W. Tsai, and Y. Meurice, *Phys. Rev. A* **96**, 023603 (2017), arXiv:1611.05016 [cond-mat.quant-gas].
- [23] Y. Meurice, “Supplementary material,” (2024).
- [24] J. Wurtz, A. Bylinskii, B. Braverman, J. Amato-Grill, S. H. Cantu, F. Huber, A. Lukin, F. Liu, P. Weinberg, J. Long, S.-T. Wang, N. Gemelke, and A. Keesling, “Aquila: Quera’s 256-qubit neutral-atom quantum computer,” (2023), arXiv:2306.11727 [quant-ph].
- [25] H. Bernien, S. Schwartz, A. Keesling, H. Levine, A. Omran, H. Pichler, S. Choi, A. S. Zibrov, M. Endres, M. Greiner, V. Vuletić, and M. D. Lukin, *Nature* **551**, 579 (2017).
- [26] A. Keesling, A. Omran, H. Levine, H. Bernien, H. Pichler, S. Choi, R. Samajdar, S. Schwartz, P. Silvi, S. Sachdev, P. Zoller, M. Endres, M. Greiner, V. Vuletić, and M. D. Lukin, *Nature* **568**, 207 (2019).
- [27] H. Labuhn, D. Barredo, S. Ravets, S. de Léséleuc, T. Macrì, T. Lahaye, and A. Browaeys, *Nature* **534**, 667 (2016).
- [28] S. de Léséleuc, V. Lienhard, P. Scholl, D. Barredo, S. Weber, N. Lang, H. P. Büchler, T. Lahaye, and A. Browaeys, *Science* **365**, 775 (2019).
- [29] S. Ebadi, T. T. Wang, H. Levine, A. Keesling, G. Semeghini, A. Omran, D. Bluvstein, R. Samajdar, H. Pichler, W. W. Ho, S. Choi, S. Sachdev, M. Greiner, V. Vuletić, and M. D. Lukin, *Nature* **595**, 227 (2021).
- [30] P. Scholl, M. Schuler, H. J. Williams, A. A. Eberharter, D. Barredo, K.-N. Schymik, V. Lienhard, L.-P. Henry, T. C. Lang, T. Lahaye, A. M. Läuchli, and A. Browaeys, *Nature* **595**, 233 (2021).
- [31] J. Zhang, S. H. Cantú, F. Liu, A. Bylinskii, B. Braverman, F. Huber, J. Amato-Grill, A. Lukin, N. Gemelke, A. Keesling, S.-T. Wang, Y. Meurice, and S. W. Tsai, “Probing quantum floating phases in rydberg atom arrays,” (2024), arXiv:2401.08087 [quant-ph].
- [32] This was pointed out to us by Alex Lukin.
- [33] A. Lukin, M. Rispoli, R. Schittko, M. E. Tai, A. M. Kaufman, S. Choi, V. Khemani, J. Léonard, and M. Greiner, *Science* **364**, 256–260 (2019).
- [34] G. Torlai, B. Timar, E. P. van Nieuwenburg, H. Levine, A. Omran, A. Keesling, H. Bernien, M. Greiner, V. Vuletić, M. D. Lukin, R. G. Melko, and M. Endres, *Physical Review Letters* **123** (2019), 10.1103/physrevlett.123.230504.
- [35] J. Zhang, J. Unmuth-Yockey, J. Zeiher, A. Bazavov, S.-W. Tsai, and Y. Meurice, *Phys. Rev. Lett.* **121**, 223201 (2018).
- [36] F. M. Surace, P. P. Mazza, G. Giudici, A. Lerosé, A. Gambassi, and M. Dalmonte, *Phys. Rev. X* **10**, 021041 (2020).
- [37] S. Notarnicola, M. Collura, and S. Montangero, *Phys. Rev. Res.* **2**, 013288 (2020).
- [38] A. Celi, B. Vermersch, O. Viyuela, H. Pichler, M. D. Lukin, and P. Zoller, *Phys. Rev. X* **10**, 021057 (2020), arXiv:1907.03311 [quant-ph].
- [39] Y. Meurice, *Phys. Rev. D* **104**, 094513 (2021), arXiv:2107.11366 [quant-ph].
- [40] P. Fromholz, M. Tsitsishvili, M. Votto, M. Dalmonte, A. Nersisyan, and T. Chanda, *Phys. Rev. B* **106**, 155411 (2022).
- [41] D. González-Cuadra, T. V. Zache, J. Carrasco, B. Kraus, and P. Zoller, *Phys. Rev. Lett.* **129**, 160501 (2022), arXiv:2203.15541 [quant-ph].
- [42] K. Heitritter, Y. Meurice, and S. Mrenna, (2022), arXiv:2212.02476 [quant-ph].
- [43] C. W. Bauer *et al.*, *PRX Quantum* **4**, 027001 (2023), arXiv:2204.03381 [quant-ph].
- [44] J. C. Halimeh, M. Aidelsburger, F. Grusdt, P. Hauke, and B. Yang, (2023), arXiv:2310.12201 [cond-mat.quant-gas].
- [45] J. Zhang, S.-W. Tsai, and Y. Meurice, (2023), arXiv:2312.04436 [quant-ph].
- [46] R. D. Pisarski, V. V. Skokov, and A. M. Tsvetik, *Universe* **5**, 48 (2019).
- [47] T. Kojo, Y. Hidaka, L. McLerran, and R. D. Pisarski, *Nuclear Physics A* **843**, 37 (2010).
- [48] M. Headrick and T. Takayanagi, *Phys. Rev. D* **76**, 106013 (2007), arXiv:0704.3719 [hep-th].
- [49] P. Hayden, M. Headrick, and A. Maloney, *Phys. Rev. D* **87**, 046003 (2013), arXiv:1107.2940 [hep-th].
- [50] T.-C. Lin and J. McGreevy, *Phys. Rev. Lett.* **131**, 251602 (2023), arXiv:2303.05444 [hep-th].
- [51] Z. Ozzello and Y. Meurice, “Work in progress,” (2024).
- [52] M. Asaduzzaman, S. Catterall, A. Maloney, Y. Meurice, A. Samlodia, and G. C. Toga, “Work in progress,” (2024).
- [53] J. Corona, M. Asaduzzaman, and Y. Meurice, “Work in progress,” (2024).

Supplementary Material

In this supplementary material we provide more information about:

- I. Experimental methods
- II. Additional information

- A. Bi-partite Hilbert space
- B. Detailed features of Fig. 1
- C. Entropy errors
- D. Verification of the bound for two qubits
- E. Other examples
- F. Second-order Renyi entropies

I. EXPERIMENTAL METHODS

Analog calculations with arrays of Rydberg atoms have been performed with Aquila using the Amazon Braket services. We used the Amazon Braket SDK for local simulations. This imposes constraints not present in exact diagonalization. Analog calculations were performed with a single chain model with 10 sites, $\Omega = 5\pi$ MHz, which implies $R_b = 8.375\mu$, and a detuning $\Delta = 17.5\pi$ MHz. The linear size of the system needs to be less than $100 \mu\text{m}$. This means that we need $R_b/a_x \gtrsim 0.9$. The distance between the atoms needs to be more than $4 \mu\text{m}$ which implies $R_b/a_x \lesssim 2.0$. We used the values $R_b/a_x = 0.9, 1.0, \dots, 2.0$. The ground state needs to be prepared adiabatically and actual measurements with Aquila are performed after turning off Ω . The procedure suggested on the Amazon Braket tutorials lasts $4 \mu\text{s}$ and involves ramping down Ω during the last $0.5 \mu\text{s}$, as illustrated in Fig. 5. We used 1000 shots 10 times for the local simulator and had 2 runs with 1000 shots for Aquila.

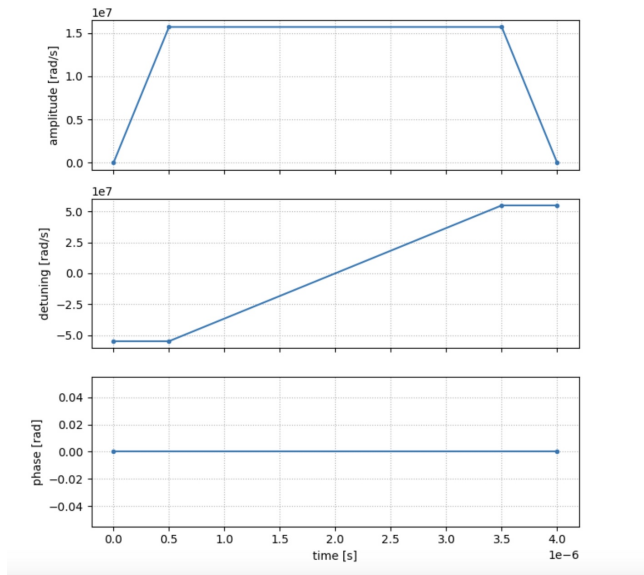


FIG. 5. Standard ramping up or down of Ω (top), Δ (middle) and ϕ (bottom) as provided by the Amazon Braket.

II. ADDITIONAL INFORMATION

Bi-partite Hilbert space

In the following we consider N_q two-state systems (qubits), for instance an array of Rydberg atoms either in the ground $|g\rangle$ or Rydberg $|r\rangle$ state. For simplicity, we assume that N_q is even and that the whole system (AB) can be divided in two subsystems A and B that can be mapped into each other by some reflection symmetry. A simple example is a linear chain of equally spaced Rydberg atoms with an even number of atoms.

The computational basis consists of the 2^{N_q} elements

$$|\{n\}\rangle \equiv |n_0, n_1, \dots, n_{N_q-1}\rangle, \quad (13)$$

with $n_j = 0$ or 1 . Any element of this basis can be factored in a bi-partite way with the two subsystems of identical size A and B (each with $N_q/2$ qubits)

$$|\{n\}_{AB}\rangle = |\{n\}_A\rangle |\{n\}_B\rangle, \quad (14)$$

with

$$|\{n\}_A\rangle \equiv |n_0, n_1, \dots, n_{N_q/2-1}\rangle \text{ and} \quad (15)$$

$$|\{n\}_B\rangle \equiv |n_{N_q/2}, \dots, n_{N_q-1}\rangle \quad (16)$$

Given an arbitrary prepared state $|\psi\rangle$, we can expand it in the computational basis

$$|\psi\rangle = \sum_{\{n\}} c_{\{n\}} |\{n\}\rangle, \quad (17)$$

and the state $|\{n\}\rangle$ will be observed with a probability

$$p_{\{n\}} = |c_{\{n\}}|^2. \quad (18)$$

These probabilities can be estimated by measurements and define an “experimental” entropy

$$S_{AB}^X \equiv - \sum_{\{n\}} p_{\{n\}} \ln(p_{\{n\}}), \quad (19)$$

associated with the state $|\psi\rangle$. It is clear that this quantity depends on the computational basis and that it contains no information about entanglement.

We now define a reduced probability in the subsystem A by tracing over B :

$$p_{\{n\}_A} = \sum_{\{n\}_B} p_{\{n\}_A \{n\}_B}, \quad (20)$$

and the corresponding reduced entropy

$$S_A^X \equiv - \sum_{\{n\}_A} p_{\{n\}_A} \ln(p_{\{n\}_A}). \quad (21)$$

Again, this quantity depend on the computational basis used and cannot be identified with the von Neuman entropy S_A^{vN} .

In the following we focus on the case where $|\psi\rangle = |vac.\rangle$, the vacuum of the Hamiltonian. Starting with

$$\rho_{AB} = |vac.\rangle \langle vac.|\quad (22)$$

and writing the 2^{N_q} dimensional vector $c_{\{n\}}$ corresponding to the vacuum as a $2^{N_q/2} \times 2^{N_q/2}$ matrix

$$C_{\{n\}_A, \{n\}_B} = c_{\{n\}}, \quad (23)$$

we find that the reduced density matrix $\rho_A = Tr_B \rho_{AB}$ can be written as

$$\rho_{A\{n\}_A, \{n'\}_A} = (CC^\dagger)_{\{n\}_A, \{n'\}_A}, \quad (24)$$

in the computational basis. The von Neuman entropy is

$$S_A^{vN} = - \sum_m \lambda_m \ln(\lambda_m), \quad (25)$$

with λ_m the eigenvalues of ρ_A which are independent of the basis used in A .

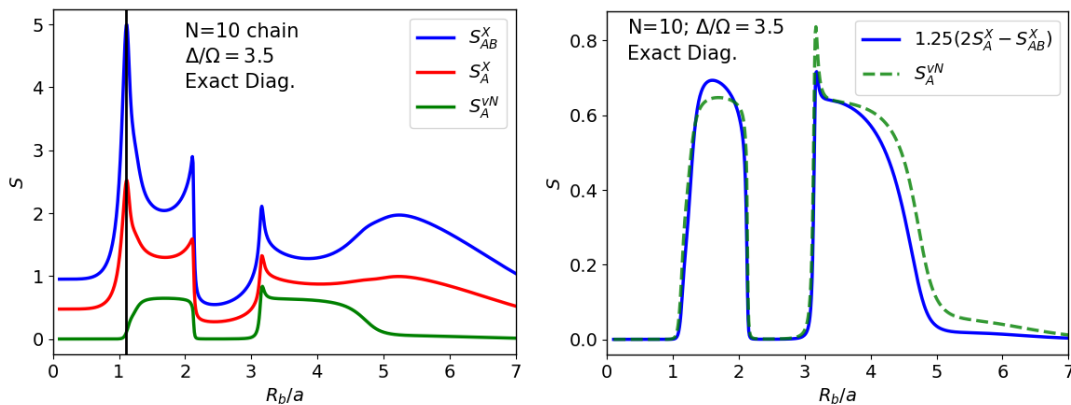


FIG. 6. Entropies for a chain of 10 atoms with $\Delta/\Omega = 3.5$ as a function of R_b/a_x . Top: S_{AB}^X , S_A^X and S_A^{vN} ; the vertical line is at $R_b/a_x = 1.11$; Bottom: $1.25(2S_A^X - S_{AB}^X)$ and S_A^{vN} .

Detailed features of Fig. 1 (in the main text)

Several features of Fig. 6 (here, Fig. 1 in the main text) can be understood from elementary considerations. For $R_b/a_x = 0.5$, we have essentially 10 decoupled atoms. Each of the single-atom ground states have a probability $\cos(\theta/2)^2 = 0.981$ (with $\theta = \arctan(\Omega/\Delta)$) to be in the $|r\rangle$ state and the entropy per atom is 0.0951. Numerically we found $S_{AB}^X = 0.9616 \simeq 2S_A^X$ with 3 significant digits while S_A^{vN} is negligible. Near $R_b/a_x=1$, S_{AB}^X and S_A^X increase rapidly to reach maxima near $R_b/a_x = 1.1$ with $S_{AB}^X = 4.874 \simeq 2S_A^X = 4.901$. The most probable state is $|rrrrrrrrrr\rangle$ with a probability of 0.036. For $R_b/a_x = 1.5$, there are four states with probabilities larger than 0.1: $|rggrgrgrgr\rangle$, $|rgrgrgrgrgr\rangle$ (0.138) and $|rgrgrgrgrgr\rangle$ $|rgrgrgrgrgr\rangle$ (0.276). After tracing over the right part, there are three significant probabilities for $|rggrg\rangle$, $|rgrgg\rangle$, and $|rgrgr\rangle$ and $2S_A^X - S_{AB}^X = 0.549$ while $S_A^{vN} = 0.638$. For $R_b/a_x = 2.5$, the state $|rggrgrgrgr\rangle$ has a probability 0.888 and both $2S_A^X - S_{AB}^X$ and S_A^{vN} are small.

Entropy errors

In this supplemental information section, we compare the errors for the local simulator with no ramping down (LSNRD), the local simulator with the standard ramping down (LSST) as in Fig. 5, and the actual device Aquila.

We started with the local simulator and found some dependence on the details of the ramping down of Ω at the end. The local simulator allows us to try time sequences not possible with the actual device. In order to check that the adiabatic preparation is working well, we first considered the situation with $\Omega(t)$ flat at the end (so 5π MHz after 4μ sec instead of ramping down to zero after 3.5μ s as in Fig. 5). We used 1000 shots and repeated the experiment ten times in order to estimate the statistical errors. The results are shown in Fig. 7 and show good agreement with exact diagonalization. Except for $R_b/a_x = 1.1, 1.2$ and 2.0 , the values $1.25(2S_A^X - S_{AB}^X)$ obtained with the local simulator agree with less than one standard deviation with the exact diagonalization results. This gives us confidence in the adiabatic preparation of the ground state.

We repeated the local simulation with the realistic ramping down at the end shown in Fig. 5. The results are shown in Fig. 8. The agreement is not as good as in Fig. 7. The size of the statistical errors bars are much smaller than the discrepancies with exact diagonalization for S_{AB}^X and S_A^X . However the error somehow cancel in $2S_A^X - S_{AB}^X$ and we obtain reasonable estimates of S_A^{vN} .

We repeated parts of these simulations with the actual device and we can now compare the estimations of S_{AB}^X and S_A^X obtained with: 1) exact diagonalization, 2) the local simulator with no ramping down (LSNRD) as in Fig. 7, 3) the local simulator with the standard ramping down (LSST) as in Fig. 8, and 4) the actual device Aquila. We focus the discussion on $R_b/a_x = 1.5$. In cases 2), 3) and 4) we used two independent runs with 1000 shots. By dividing the number of events by 1000, we obtain estimations of the probabilities that can be calculated exactly.

The results involving more than 10 counts are shown in Table I and lead to the conclusions that:

- LSNRD provides reasonably accurate estimations of the probabilities for states in the computational basis, for a broad range of values for the probabilities. This is not a surprise, it just shows that the local simulator works properly.

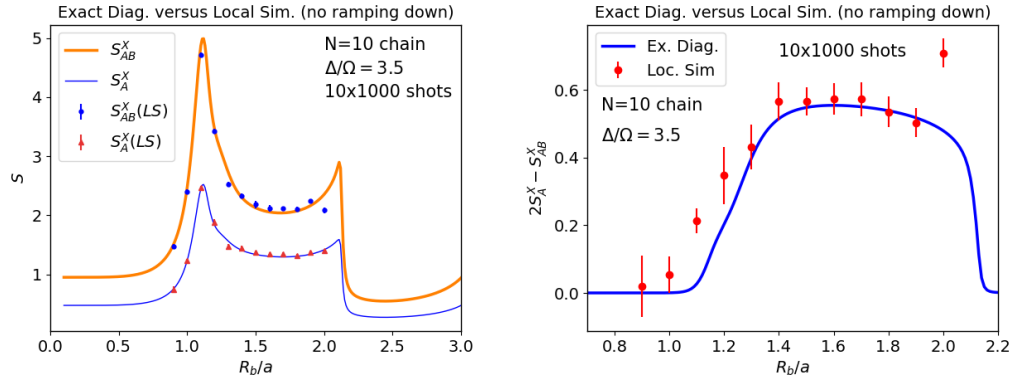


FIG. 7. Left: S_{AB}^X and S_A^X vs. R_b/a_x with exact diagonalization (continuous curves) and the local simulator with no ramping down of Ω at the end (symbols) using 1000 shots 10 times. The errors bars are present but barely visible on the graph. Right: $1.25(2S_A^X - S_{AB}^X)$ with the same conventions. As the vertical scale is five times smaller, the errors bars are clearly visible.

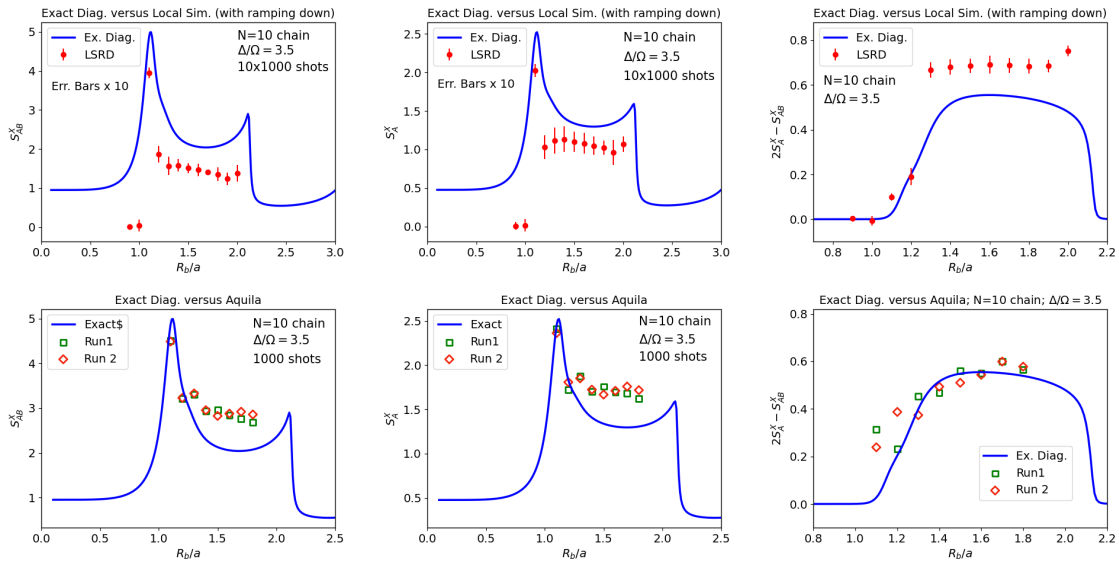


FIG. 8. Top: S_{AB}^X (left), S_A^X (middle) and $2S_A^X - S_{AB}^X$ (right) vs. R_b/a_x with exact diagonalization (continuous curves) and the local simulator with ramping down of Ω at the end as in Fig. 5 (symbols) using 1000 shots 10 times. The errors bars are multiplied by 10. Bottom: same quantities with Aquila with 2 runs of 1000 shots.

- LSST removes states with low probabilities and significantly amplifies some medium probabilities such as 0.138 for rgrgrgrgr and rgrgrgrgr. This suggests that a more rapid ramping down maybe preferable for entropy estimation.
- Aquila amplifies some of the low probability states and depletes higher probability states while keeping some ratios roughly in line with exact results.

From the above discussion, it is clear that there are significant fluctuations for states that are expected to be seen 10 times or less in 1000 shots. LSST removes these states while Aquila amplifies them. This suggests to discard results with low counts and proceed with truncated data sets. In the following we considered truncated data sets where states with 10 or less measurements were discarded. By doing this, the number of shots is reduced which leads to different probability estimates. The results of this truncation for the entropies are shown in Table II. From these results we conclude that

- The truncation lowers the entropies calculated with exact diagonalization by about 20 percent but increases $1.25(2S_A^X - S_{AB}^X)$ by about 10 percent.

- LSNRD follows closely the exact results. Again this was expected.
- LSST is insensitive to the truncation. The LSST values are close to exact truncated values. Again this was expected.
- Aquila results are very sensitive to truncation which brings the results closer to exact ones, but maybe not as close as hoped.

More generally, the truncation method seems to introduce significant uncertainties and we believe that error cancellations with the untruncated procedure may be more reliable.

Method State	Exact	LSNRD1	LSNRD2	LSST1	LSST2	Aquila1	Aquila2
grgrgrgrgr	12	14	19	24	18	16	18
rggggrgrgr	16	21	18	< 10 (0)	< 10 (1)	15	14
rggrgrgrgr	138	142	152	201	222	136	149
rgrgggrgr	23	18	28	< 10 (0)	< 10 (0)	19	24
rgrgrgrgg	< 10 (6)	11	< 10 (7)	< 10 (0)	< 10 (0)	14	< 10 (5)
rgrgrgrgr	276	232	239	274	264	174	175
rgrrggggr	16	14	18	< 10 (0)	< 10 (0)	19	12
rgrgrgrgr	276	248	244	278	266	190	180
rgrgrgrgr	138	179	168	207	200	151	179
rgrgrgrgrg	12	13	18	12	25	23	16
Total	907	892	904	996	995	804(*)	812(**)

TABLE I. States with at least 10 observations for 1000 shots. For Aquila, (*) five additional states are not in the table: ggrgrgrgr (12), rgggrgrgr (12), rggrgrgggr (12), rgrgrgggr (14), rgrgrgrrr (11) for run 1, and (**) and three additional states are not in the table: rgggrgrgr (12), rgrgggrgr (11), rgrgrgggr (12) for run 2.

Method Entropy	Exact	LSNRD1	LSNRD2	LSST1	LSST2	Aquila1	Aquila2
S_{AB}^X	2.126	2.241	2.198	1.527	1.558	2.944	2.874
$S_{AB}^X(\text{Trunc.})$	1.6476	1.734	1.740	1.504	1.527	2.035	1.901
S_A^X	1.337	1.374	1.354	1.117	1.134	1.685	1.681
$S_A^X(\text{Trunc.})$	1.131	1.149	1.167	1.115	1.108	1.288	1.233
$1.25(2S_A^X - S_{AB}^X)$	0.686	0.634	0.639	0.883	0.888	0.531	0.611
$1.25(2S_A^X - S_{AB}^X)(\text{Trunc.})$	0.769	0.706	0.742	0.907	0.861	0.676	0.707

TABLE II. Entropies calculated with the full data set and truncated data sets (Trunc.) where observations with less than 10 events are discarded.

Verification of the bound for two qubits

In this section, we consider a general two-qubit state

$$|\psi\rangle = \sum_{n_1 n_2=0,1} c_{n_1 n_2} |n_1 n_2\rangle. \quad (26)$$

The reduced two by two density matrix can be calculated exactly and we obtain

$$S_A^{vN} = - \sum_{\pm} \lambda_{\pm} \ln(\lambda_{\pm}), \quad (27)$$

with

$$\lambda_{\pm} = \frac{1}{2}(1 \pm \sqrt{1 - 4\text{Det}}), \quad (28)$$

with the determinant

$$\text{Det} = p_{01}p_{10} + p_{00}p_{11} - 2\sqrt{p_{00}p_{11}p_{01}p_{10}} \cos(\xi), \quad (29)$$

and a complex phase

$$\exp(i\xi) = (c_{00}c_{11}c_{01}^*c_{10}^*)/|c_{00}c_{11}c_{01}c_{10}|. \quad (30)$$

Det increases when ξ increases from 0 to π . $S_A^{vN} = 0$ when Det=0 and $\ln 2$ when Det=1/4 and in general increases with Det. Consequently, we have the inequality

$$S_A^{vN}(p_{\{n\}}, \xi) \geq S_A^{vN}(p_{\{n\}}, \xi = 0). \quad (31)$$

The inequality

$$S^{vN}(|c_{n_1 n_2}|, \xi = 0) \geq 2S_A^X - S_{AB}^X. \quad (32)$$

is verified numerically in Fig. 9 (Fig. 4 in the main text) using spherical coordinates to parametrize the norms of the coefficients expressed in spherical coordinates $|c_{00}| = \cos \phi \sin \theta$; $|c_{11}| = \sin \phi \sin \theta$; $|c_{01}| = |c_{10}| = \cos \theta / \sqrt{2}$ with $0 \leq \theta, \phi \leq \pi/2$. This enforces the constraint that the probabilities add to one.

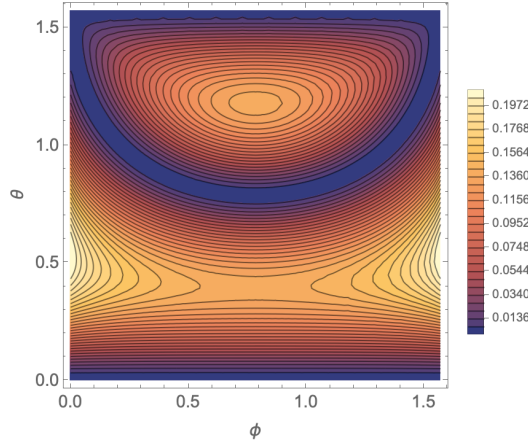


FIG. 9. $S^{vN}(\xi = 0) - (2S_A^X - S_{AB}^X)$ for two qubits using the spherical coordinates described in the text.

Other examples

We repeated the calculation for ladder-shaped arrays with 5 rungs and 2 legs and different aspect ratios. We found very similar results for the same approximate constant 1.25 as shown in Fig. 10. Fig. 11 makes clear that the inequality

$$S_A^{vN} \geq 2S_A^X - S_{AB}^X, \quad (33)$$

holds.

Second-order Rényi entropies

The equivalent of Fig. 6 for the second order Rényi entropies are displayed in Fig. 12.

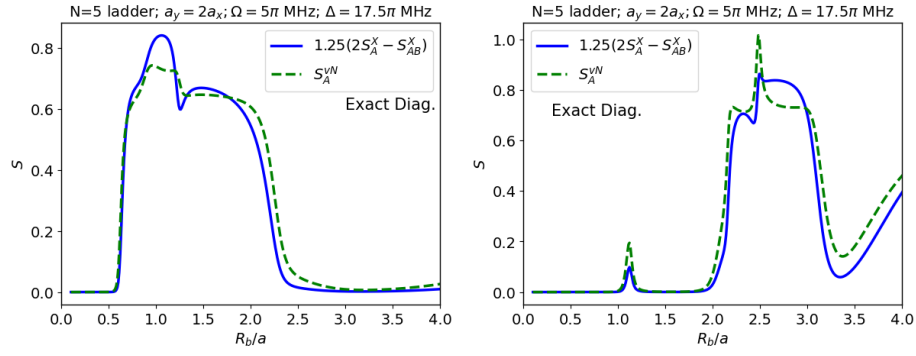


FIG. 10. $1.25(2S_A^X - S_{AB}^X)$ and S_A^{vN} as a function of R_b/a_x for $a_y = 0.5a_x$ (left) and $a_y = 2a_x$ (right).

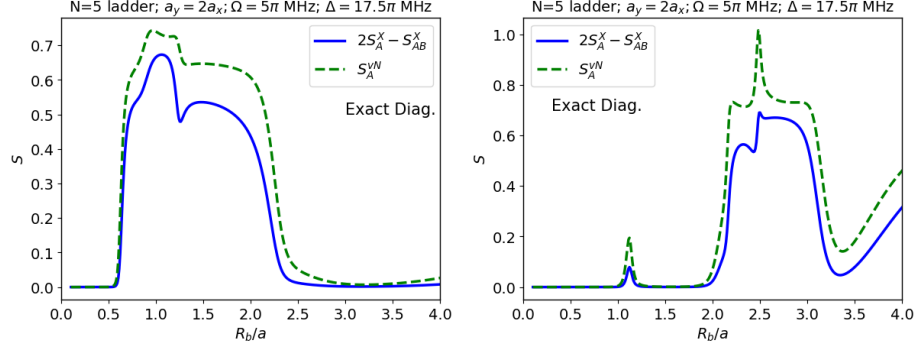


FIG. 11. $2S_A^X - S_{AB}^X$ and S_A^{vN} as a function of R_b/a_x for $a_y = 0.5a_x$ (left) and $a_y = 2a_x$ (right).

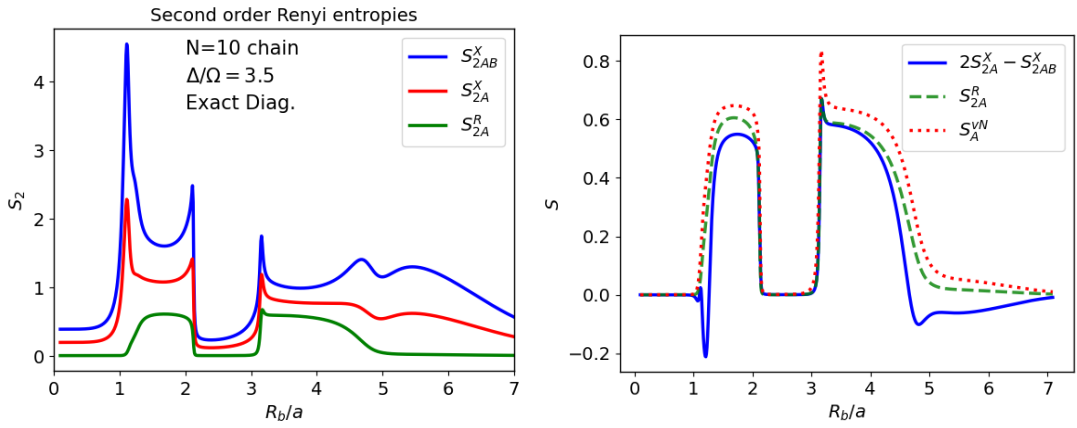


FIG. 12. Second order Rényi entropies. Left: S_{2AB}^X (top), S_{2A}^X (middle) and S_{2A}^R (bottom); Right: $2S_{2A}^X - S_{2AB}^X$, S_{2A}^R , and S_A^{vN} for a chain of 10 atoms with $\Delta/\Omega = 3.5$ as a function of R_b/a_x .